Lateral-torsional buckling design for pultruded FRP beams

T.T. Nguyen[a], T.M. Chan[*,b], J.T. Mottram[c]

[a] *Faculty of Transportation Engineering, Ho Chi Minh University of Transport, Ho Chi Minh, Vietnam*

[b]*Department of Civil and Environmental Engineering, The Hong Kong Polytechnic University, Hung Hom, Kowloon, Hong Kong*

[c]*School of Engineering, University of Warwick, Coventry, CV4 7AL, United Kingdom*

ABSTRACT

This paper presents an investigation into the development of a design procedure for Pultruded Fibre Reinforced Polymers (PFRP) beams failing by the elastic buckling mode of Lateral-Torsional Buckling (LTB). The design procedure is based on the European design approach for uniform members in bending of structural steel. In particular, the calibration method adopts the general case 'resistance' formula in Eurocode 3 (EN 1993-1-1:2005), and follows a standard design from testing procedure given in Eurocode 0 (EN 1990:2002) when calibrating the 'design model' to determine the partial factor γ_{M} for a member instability check. The test population for calibration has 114 LTB buckling resistances using four PFRP section sizes of I and channel shapes. The non-dimensional slenderness parameter is defined using the local flange buckling strength instead of the yield strength. An imperfection factor of 0.34 and partial factor of 1.3 are shown to be appropriate for calculation of the LTB moment of resistance.

Keywords: *Lateral-torsional buckling, plateau length, imperfection factor, partial factor*

* Corresponding author. Tel: +852 2766 6013
Email: thuy.nguyen@hcmutrans.edu.vn (T.T.Nguyen); tak-ming.chan@polyu.edu.hk (T.M.Chan); J.T.Mottram@awrwick.ac.uk (J.T.Mottram).

1. INTRODUCTION

Pultruded Fibre-Reinforced Polymers (PFRP) shapes consist of thin walls of E-glass fibre reinforcement embedded in a thermoset resin based matrix. They are produced by the continuous composite material process known as '*pultrusion*' [1]. Pultrusion is a cost-effective process that can be employed to produce a wide range of uniform cross-section shapes suitable for use in civil engineering strucutres [1]. Fibre reinforcement comprises of alternate layers of unidirectional rovings and a mat, the latter is usually of continuous fibres having a random distribution in the plane. The outer layers in the PFRP shape are always of mat reinforcement [1-3]. E-glass fibres provide strength and stiffness, while the matrix creates the shape and enables load transfer into the fibres. The mechanical properties of the polymeric composite material are orthotropic, with the higher strengths and stifnesses in the direction of pultrusion. Distinct advantages, such as lightweight (about ¼th of steel), relative high tensile strength of 200 MPa to 400 MPa, corrosion resistant and electro-magnetic transparent make this emerging structural material attractive for applications benefiting from its engineering properties [1].

Although PFRP structural shapes are found in building and bridge structures, the currently lack of recognised design guidance [2] is inhibiting their wider exploitation. In this paper the authors present a complete calibration for a procedure to predict the resistance (strength) of PFRP members in bending that fail with the elastic mode of Lateral-Torsional Buckling (LTB). The experimental test results for this calibration study are reported and discussed in references [4] and [5].

2. LTB DESIGN FOR STEEL MEMBERS

LTB is a key instability mode of ultimate failure for flexure actions about the major-axis of open sections, which for beams could be of I, H or C shapes. It is characterised by a

coupled elastic (small displacement) deformation of lateral deflection and twist about the beam's longitudinal axis; there is no cross-sectional distortion. When designing a frame structure of PFRP shapes, a laterally unrestrained beam subject to major axis bending has to be verified for resistance against the Ultimate Limit State (ULS) failure mode of LTB [6]. This section will present the current design methodology adopted in American and Eurocode design standards for steel beams, and pave the way for the subsequent discussion towards a design procedure for equivalent PFRP members in bending using the Eurocode approach.

2.1 American Approach

Design standard AISC 360, giving the Specification for Structural Steel Buildings [7], follows the North American limit state approach of Load and Resistance Factor Design (LRFD). This steel standard, in Chapter F for Design of Members for Flexure states that:

$$M_{\mathrm{u}} \le \phi_{\mathrm{b}} M_{\mathrm{n}} \tag{1}$$

where M_{u} is the required flexural strength (or 'design moment') calculated using the LRFD load combinations; M_{n} is the nominal flexural strength and $\phi_{\mathrm{b}} = 0.9$ is the resistance factor for flexure (bending). Note that the resistance factor serves the same purpose as $1/\gamma_{\mathrm{M1}}$ in Eurocode 3 Part 1-1 [5] where γ_{M1} is the partial factor for resistance of members to instability assessed by member checks; their values can be different because the calibration methods are not identical.

LTB strength depends on the member's lateral unsupported length, L_{b}, which is the abscissa axis in Fig. 1, for a plot of how M_{n} varies with this length. If L_{b} is less than, or equal to the limiting laterally unbraced length for the limit state of steel yielding, L_{p}, no LTB check is required. When L_{b} lies between L_{p} and the limiting laterally unbraced

length, L_r, for inelastic LTB, the design process must take into account the inelastic response of steel. When $L_b > L_r$, M_n is equal to M_{cr}, where M_{cr} is the elastic critical buckling moment for LTB failure.

There is an American pre-standard for the LRFD of PFRP structures [8] that has adopted a similar approach to what is established in AISC 360. One necessary revision is that the pre-standard has incorporated an additional time-effect factor λ in evaluating the flexural resistance from:

$$M_u \leq \lambda \phi M_n \tag{2}$$

λ (≤ 1.0) takes into account the long-term response of FRP, such as from creep and the reduction in mechanical properties from exposure to aggressive environments [8]. The resistance factor ϕ for LTB failure is taken in the pres-standard to be 0.7, to reflect the greater uncertainty in quantifying the 'true' behaviour and the higher target reliability factor (β) than that deemed acceptable for steel [8].

2.2 Eurocode Approach

The primary design approach in Eurocode 3 Part 1-1(EN 1993-1-1:2005) [9] adopts the form of LTB curve shown in Fig. 2 when establishing resistance of laterally unrestrained uniform steel members subject to flexure about the major *y-y* axis. For the beam to pass the LTB design check of Clauses 6.3.2, its design buckling resistance moment, $M_{b,Rd}$, must be higher than the design bending moment about the *y-y* axis, $M_{y,Ed}$. $M_{b,Rd}$ can be evaluated as follows:

$$M_{b,Rd} = \chi_{LT} W_y f_y / \gamma_{M1} \tag{3}$$

where χ_{LT} is the reduction factor for LTB (≤ 1.0); W_y is the appropriate section modulus about the major axis, f_y is the yield strength and γ_{M1} is the partial factor for resistance of members to instability and is taken as 1.0.

χ_{LT} is derived from the solution to the Ayrton-Perry Formula (APF) [10]. For the general case, the LTB curve is defined by:

$$\chi_{LT} = \frac{1}{\Phi_{LT} + \sqrt{\Phi_{LT}^2 - \bar{\lambda}_{LT}^2}} \tag{4}$$

where $$\Phi_{LT} = 0.5\left[1 + \alpha_{LT}\left(\bar{\lambda}_{LT} - \bar{\lambda}_{LT,0}\right) + \bar{\lambda}_{LT}^2\right], \tag{5}$$

To complete the curve shown in Fig.2, $\bar{\lambda}_{LT,0}$ is for the plateau length when χ_{LT} is always equal to 1.0.

Φ_{LT} can be expressed in a form of a generalized imperfection factor η_{LT} as [10]:

$$\Phi_{LT} = 0.5\left(1 + \eta_{LT} + \bar{\lambda}_{LT}^2\right) \tag{6}$$

where the non-dimensional slenderness $\bar{\lambda}_{LT}$ is given by:

$$\bar{\lambda}_{LT} = \sqrt{\frac{W_y f_y}{M_{cr}}} \tag{7}$$

The imperfection factor α_{LT} for (steel) buckling curves can be taken as 0.21, 0.34, 0.49 or 0.76 for different cross-section shapes and geometric dimensions.

There is currently no Eurocode standard for the design of pultruded FRP structures. A report in 2007 by Gutiérrez *et al*. [11] introduces a plan for its preparation. To provide supportive information to its 'code' writers this paper proposes a generic LTB curve for uniform PFRP members in bending that is calibrated against the Eurocode framework. The key calibrations are carried out to establish the three design parameters of: (1) plateau length, $\bar{\lambda}_{LT,0}$; (2) imperfection factor, α_{LT} and (3) partial factor, γ_{M1} (which in this paper will be γ_M).

3. EVALUATION OF M_{cr} AND MATERIAL CHARACTERIZATION FOR PULTRUDED FRP BEAMS

3.1 Evaluation of M_{cr}

Theoretical investigations on LTB have been a subject of research for more than eight decades [12-16]. These contributions have resulted in a general closed-form expression for elastic critical buckling moment M_{cr} of an isotropic beam that has a symmetrical cross-section about the *y-y* axis. This expression allows for different bending moment distributions, changing end support and warping restraints, as well as different heights at which the loading is applied. It can be written as [14, 16-17]:

$$M_{cr} = C_1 \frac{\pi^2 E I_z}{L_{cr}^2} \left\{ \left[\left(\frac{k}{k_w} \right)^2 \frac{I_w}{I_z} + \frac{L_{cr}^2 G I_T}{\pi^2 E I_z} + \left(C_2 z_g \right)^2 \right]^{0.5} - C_2 z_g \right\} \quad (8)$$

In Eq. (8) L is the member's span; C_1 is the equivalent uniform moment factor that accounts for the shape of the bending moment distribution; C_2 is the factor to account for the vertical load height with respect to the Shear Center (SC); z_g is the height of the load from the SC (z_g = 0 when the load is applied at the shear center), and is positive when the load is located above and is negative when placed below; I_z, I_w and I_T are the second moment of area for flexure about the beam's minor axis, warping constant and torsional constant; k and k_w are the effective length factors for lateral flexure and warping, respectively.

Eq. (8) is adopted in Eurocode 3 [9] to evaluate $\bar{\lambda}_{LT}$ through Eq. (7). Both the American AISC 360 [7] and FRP pre-standard [8] assume the same (safe) approximation by taking the effective length factors k and k_w to be 1.0. The difference in the modelling of isotropic and orthotropic materials is related to the stress-strain relationships for elastic constants [18]. By replacing the isotropic moduli of elasticity with the orthotropic

equivalents [19] in Eq. (8) and, when required, taking account of the influence of shear deformation, an expression for M_{cr} for FRP beams is established [6]. The presence of shear deformability will slightly reduce, say by < 5%, the critical elastic moment of resistance for a narrow-flange PFRP beam (e.g. with flange outstand equal to half section depth). Because shearing is unlikely to reduce M_{cr} by 10% it is neglected herein, and, as recommended by others [6, 18, 20-21], Eq. (8) is used for PFRP members in bending after substituting E with the Longitudinal modulus of elasticity, E_L, and G with the in-plane shear modulus G_{LT} for an FRP material.

3.2 Material characterization

In the series of LTB tests [4-5] four PFRP shapes were used and their cross-section dimensions are defined in Fig. 3. One is an I-shape and the other three were different sized channels (labelled C1 to C3). The cross-section geometries were measured and mean values used in standard formulae to establish the geometric properties of I_z, I_T and I_W. These are reported in Table 1of reference [5].

E_L for each of the four PFRP shapes was determined using standard tensile coupon testing in accordance with BS EN 527-1 [22] and BS EN 527-4 [23]. Full details on the material characterization work are to be found in reference [4]. The hatched areas in Fig. 3 (with labels) are for the coupon locations. For the single I-shape there were six coupons around its cross-section, while there were four coupons with the three channel shapes. Coupons were taken at three cross-sections along the length of a section. There was a total of 18 coupons for the I shape and 12 for each channel. To determine the tensile E_L two axial strain gauges were attached at mid-length and the load-strain histories were recorded using real time data acquisition [4].

Plotted in Fig. 4 is a typical stress-strain curve. BS EN 527-1 requires E_L to be determined from stresses for direct strain (ε_L) readings between 0.05% and 0.25%. E_L can be established, via either the chord modulus between a start point (i.e. ε_L = 0.05%) and end point (i.e. ε_L = 0.25%) or the slope of the linear least-squares (best fit) line within this ε_L interval. The latter option was adopted in [4]. It is recognized that test standard BS EN 527-1 is for unreinforced plastics and was not written for tensile testing with PFRP materials. The low range of strain (up to 0.25%) might have been specified because a nonlinear response occurs at higher ε_{Ls} in an unreinforced plastic. A considerably higher maximum strain could have been chosen with a PFRP material that is subjected to tension in the pultrusion direction. Different ranges of strain were examined by Nguyen [4], and it has been found that any difference in E_L is statistically insignificant. To determine the mean E_L for Eq. (8) it was decided that the ε_L range can be taken between 0.1 and 0.5%.

The measurement of G_{LT} is more challenging [4]. The experimental problem is to have a test method with sufficient material volume in pure shear. A number of current standard test methods are found not to be satisfactory in meeting this requirement. Amongst the test methods, the more common are the: Iosipescu ASTM D5379 [24]; V-notched rail shear test ASTM D7078 [25]; plate twist method BS EN 15310 [26]; 10^o off-axis tensile test. In [4] the first author compares and contrasts these four methods for the determination of G_{LT}, and concludes that only the latter test method satisfies the material volume requirement and can be used to measure the shear strength, τ_u.

The ten-degree (10^o) off-axis method was developed in references [27] and [28] to obtain G_{LT} and τ_u for an FRP material having continuous aligned unidirectional fibres. A rectangular coupon is prepared such that the longitudinal axis of the unidirectional

fibres is at 10^o to the tensile load direction, which is parallel to the longitudinal sides of the coupon. A biaxial stress state is induced that consists of the three in-plane stresses of σ_{11} (parallel to fibres), σ_{22} (transverse to fibres) and σ_{12} (shear stress). This stress state is shown in Fig. 5, where the angle θ is 10^o. The shear stress can be expressed as [28]:

$$\tau_{12} = -\cos(\theta)\sin(\theta)\sigma_{xx} = 0.17\sigma_{xx} \quad (9)$$

where σ_{xx} is the applied tensile stress, and is load/coupon cross-sectional area.

The equivalent principal strains can be expressed, by using a transformation relationship [28], as functions of a set of three direct strains at any point. By measuring the set with a strain rosette, the shear strain γ_{12} can be found, and G_{LT} is determined from τ_{12}/γ_{12}. This test method is used in this work [4] because of its simplicity in both coupon preparation and loading, and owing to the advantage of a relatively large volume of material being subject to shearing deformation.

Because the 10^o off-axis test does not possess an ISO or ASTM standard there is no standard specification for coupon dimensions and preparation, test procedure and the strain ranges when determining G_{LT}. One option can be to test in accordance with the basic requirements in Part 5 of BS EN ISO-527 [29], since this standard provides the 'test conditions for the determination of tensile properties of unidirectional FRPs'. It requires the coupon to have dimensions of 25 mm (width) by 250 mm (length) and a thickness of 2 mm. Our coupons have a nominal size of 30 mm (width) by 300 mm (length) and a nominal wall thickness of 6 mm. A high aspect ratio (i.e. length/width =10) is employed to reduce the influence of any end constraint effect.

Five coupons were cut from the web of the shapes (I, C1 to C3) shown in Fig. 3. A rosette strain gauge was attached at the mid-point, as shown in Fig. 5, to measure the set of strains from which γ_{12} can be calculated. At the same time the applied tensile force was recorded to obtain τ_{12}. The range of shear strain for determination of G_{LT} was chosen [4] to be between 0.05% and 0.25%. Fig. 6 (a) shows a typical response of τ_{12} and γ_{12}, and Fig. 6 (b) is the zoom-in plot for γ_{12} in the strain range of 0 to 0.4%. Added in part (b) is a least-squares (best fit) straight line for the strain interval from 0.05% to 0.25%. The trend line's gradient is G_{LT} and the means from batches of five specimens for each of the four shapes are used in the γ_M calibration to follow.

Table 1 presents the two elastic constants and their corresponding statistical analysis for variation. Mean values (also taken as characteristic values in this paper) for E_L and G_{LT} are reported in columns (2) and (5) for the four shapes introduced in column (1). A batch Standard Deviation (SD) and Coefficient of Variation (CV) are reported in columns (3) and (4) for E_L and in columns (6) and (7) for G_{LT}. It is seen that the CV ranges from 1.9 to 3.9% for the Longitudinal modulus and higher at 3.0 to 8.6% for the in-plane shear modulus.

4. LTB DESGIN FOR PFRP MEMBERS IN BENDING

As discussed in Section 2 the three key design parameters (see Fig. 2) that need to be established are $\bar{\lambda}_{LT,0}$, α_{LT} and γ_M. The calibration process to be reported next is based on test results using 30 beam configurations [5] for both I and C1 shapes.

4.1 Determination of $\bar{\lambda}_{LT,0}$

First target is to determine the plateau length $\bar{\lambda}_{LT,0}$. For members with slendernesses $\bar{\lambda}_{LT} \le \bar{\lambda}_{LT,0}$, only the cross-sectional resistance check is required. For $\bar{\lambda}_{LT} > \bar{\lambda}_{LT,0}$, the elastic LTB mode of failure is to govern. EN 1993-1-1:2005 [9] assigns $\bar{\lambda}_{LT,0} = 0.2$ in the general case curves of Clause 6.3.2.2, and 0.4 in Clause 6.3.2.3 for the specific case curves for steel rolled sections and equivalent welded sections. It is worth noting that $\bar{\lambda}_{LT,0}$ is strongly influenced by the mode of failure of the cross-section. For steel it depends on classification of (steel) sections as explained in Section 5.5 of [9].

Because of the relatively high strength-to-stiffness ratios [18] it is observed that the cross-section mode of failure is often to be local flange buckling, rather than PFRP material rupture. The section moment of resistance for local instability will depend on geometry, material elastic constants and moment distribution. Because it further depends of the rotational stiffness at the junctions between the web and flange walls its determination by either a closed-form equation or physical testing is not straightforward [31, 32]. Trumpf [21] carried out experimental and numerical investigations with PFRP members in bending, and following their evaluation he proposed a plateau length of $\bar{\lambda}_{LT,0} = 0.5$. Because γ_M is insensitive to the chosen value for $\bar{\lambda}_{LT,0}$, the authors have taken Trumpf's 0.5 in their calibration study.

Taking the local flange buckling mode to be the ultimate mode of failure in PFRP beams the non-dimensional slenderness $\bar{\lambda}_{LT}$ of Eq. (7) is redefined by expression:

$$\bar{\lambda}_{LT} = \sqrt{\frac{W_y \sigma_{Loc}}{M_{cr}}} \tag{10}$$

where σ_{Loc} is the Local buckling stress at instability failure, W_y is the elastic section modulus about the *y-y* axis, and M_{cr} is given by Eq. (8). In this study σ_{Loc} was obtained

from concentrically loaded compression tests using short-column specimens. For details of this series of stud column tests consult the first author's PhD thesis [4]. From assessment of the test results it is established that σ_{Loc} is 134 MPa for the I-shape and 100 MPa for the C1-shape. It is assumed that stress σ_{Loc} is constant over the area of the compression flange outstand so that the calibration procedure can neglect the presence of a stress gradient through the section's depth (h).

4.2. Determination of α_{LT}

Next target is to consider how to establish the imperfection factor, α_{LT}. In the APF solution [10] that accounts for member geometric imperfections the generalized imperfection factor η_{LT} is expressed by an expression using the mid-span minor z-z axis out-of-straightness imperfection (v_0) and initial twist rotation (φ_0). It is given by [10]:

$$\eta_{\text{LT}} = v_0 \frac{W_y}{W_w} + \varphi_0 \frac{W_y}{W_z} - \varphi_0 \frac{GI_{\text{T}}}{M_{\text{cr}}} \frac{W_y}{W_w} \tag{11}$$

where W_z, and W_w are the elastic minor z-z axis and warping sectional moduli, respectively. W_w can be expressed in a form of:

$$W_w = I_w / \Psi_{\max} \tag{12}$$

in which $\Psi_{\max}$ is the maximum value for the cross-section's warping function. $\Psi_{\max}$ was calculated using the software ShapeBuilder [33] to be $1.79\times10^3\,\text{mm}^2$ for the I-shape and $1.91\times10^3\,\text{mm}^2$ for the C1-shape.

v_0 and φ_0 are assumed to satisfy the deformed shape for the first LTB mode, that is:

$$\frac{v_0}{\varphi_0} = \frac{M_{\text{cr}}}{N_{\text{cr,z}}} \tag{13}$$

where $N_{cr,z}$ is the Euler buckling load for minor axis flexure of a column member having simply supported ends. By taking the measured initial *z-z* axis out-of-straightness imperfection δ_{max} from [4] (and in [5]) to be v_o, φ_0 can be determined from Eq. (13). η_{LT} for a PFRP shape is determined by next substituting for these two geometric imperfections into Eq. (11).

Reported in Table 2 are beam properties needed to determine α_{LT}. Columns (1) to (7) give these properties for eight sections, comprising I and C shapes at the four lengths of 1828, 2438, 2844 and 3454 mm. The chosen four lengths are for the spans (L) in the programme of LTB resistance tests reported in [4] and [5]. The eight η_{LT}s from Eq. (13) are presented in column (8), and it is seen that for the I-section η_{LT} lies in the range of 0.18 to 0.51 and for the C1-section the range is lower at 0.05 to 0.18.

From Eqs. (5), (6) and (10) we have that:

$$\eta_{LT} = \alpha_{LT}\left(\bar{\lambda}_{LT} - \bar{\lambda}_{LT,0}\right) = \alpha_{LT}\left(\sqrt{\frac{W_y \sigma_{Loc}}{M_{cr}}} - 0.5\right). \qquad (14)$$

To give the estimations of α_{LT} reported in column (9) in Table 2 we substitute into Eq. (14) for W_y, M_{cr}, and η_{LT} from columns (4), (7) and (8), and take σ_{Loc} = 134 MPa for I beams and σ_{Loc} = 100 MPa for C1 beams. It is observed that the maximum α_{LT} is 0.26 with the I-shape and 0.11 with the C1-shape. These imperfection factors are relatively lower than for steel sections of I and C shapes, which in EN 1993-1-1:2005 [9] ranges from 0.34 to 0.76. For this calibration study, the authors decided to take α_{LT} = 0.34, because this is closest to the maximum in Table 2 of 0.26 and 0.34 is familiar to practicing engineers who are designing steel structures to Eurocode 3. An imperfection factor of 0.34 is for curve *b* in EN 1993-1-1:2005.

4.3 Determination of γ_{M1}

Presented next is the standard procedure to determine the partial safety factor for instability γ_{M1}; written in herein as γ_M. The calibration was conducted with the two separate sets of data for the I- and C-shaped members introduced in Table 2. Each set of data includes experimental resistances (r_e) from 30 physical tests with three-point loading. The test method and a discussion on the results are to be found in [4] and [5].

The calibration procedure follows nine steps for the Standard Procedure in D8.2.2 of Eurocode EN 1990:2002 [30].

Step 1: *Establish a 'design model'*

The 'design model' is for the theoretical prediction of the resistance, r_t. The chosen strength function is Eq. (3) with $\bar{\lambda}_{LT}$ defined (for PFRP members) by Eq. (10). Using EN 1990:2002 notation the expression that involves all the basic variables can be written as [30]:

$$r_t = g_{rt}(\underline{X}) = \chi_{LT}(I_T, I_W, I_y, E_L, G_{LT}, \sigma_{Loc}) \times M_{Loc}(W_y, \sigma_{Loc}) \tag{15}$$

It has the seven basic variables for a PFRP member of I_T, I_W, I_y, E_L, G_{LT}, W_y and σ_{Loc}. It is a requirement that all variables are to be measured for each individual experiment that gives a single test result. Of the seven variables, those of I_T, I_W, I_y, and W_y are section geometrical properties that can readily be calculated using measured geometric dimensions and standard expressions. These dimensions are given in full in [4] and reported in Table 3. When calculating a geometric property the contribution from having four fillet areas was ignored. Because r_t predictions for LTB resistance will be lower without the fillets it is a justified calibration approximation. Mechanical properties of E_L, G_{LT} and σ_{Loc} were not measured for each beam tested. It therefore had to be assumed that the means reported in Table 2 do not change with beam

configuration. It is worth noting that in the calibration process with steel sections these material properties are not treated as a variable [34]. This may be due to E for structural steel being statistically well-defined and consistent between different grades (such as S235 to S335 in EN 1993-1-1:2005). The situation is different with PFRP materials because their mechanical properties are not that well-known by way of copious and repetitive coupon testing. Trumpf [21] combined E_{L} with I_{z} for flexural rigidity and G_{LT} with I_{T} for shear rigidity when establishing the CV for the basic variables of I_{z} and I_{T}.

σ_{Loc} is to be taken as 134 MPa and 100 MPa for the I and C1 group of beams. In the calibration process these σ_{Loc}s are assumed to be both nominal and characteristic values. This approach is similar to that used by Sedlaeck *et al*. [34], in which a nominal value is specified to be the characteristic value for the steel yield stress (f_{y}). In [34] the CV for f_{y} (V_{fy}) is taken to be 7%. The mean ($f_{\mathrm{y,m}}$) of f_{y} is then taken to be the 2.3% fractile value from:

$$f_{\mathrm{y,m}} = f_{\mathrm{y}} \exp\left(-1.64V_{\mathrm{fy}} - 0.5V_{\mathrm{fy}}\right)^{-1} \tag{16}$$

The 'V_{fy}' in Eq. (16) is from the expression $\sqrt{V_{\mathrm{m}}^2 + V_{\mathrm{G}}^2 + V_{\mathrm{f}}^2}$, in which V_{m} is the CV for model uncertainty, V_{G} is the CV for geometry of the memebr and V_{f} is the CV for the property. An acceptable approximation for this expression can be taken to be equal to the CV for the property, which in Eq. (16) is V_{fy} for property f_{y}.

By assuming that the mean σ_{Loc} can also be taken as the 2.3% fractile value, Eq. (16) can be readily modified for PFRP shapes. To account for the greater uncertainty, the CV of $V_{\sigma\mathrm{Loc}}$ is assumed to be 10%, which is 3% higher than V_{fy} is for structural grades of steel. By applying Eq. (16), the mean σ_{Locm} is 166 MPa for the I-shape and 124 MPa for

the C1-shape. Assuming that Eq. (16) is also statistically acceptable for expressing the variation in moduli E_L and G_{LT}, we can write:

$$E_{L,m} = E_L \exp\left(-1.64V_{EL} - 0.5V_{EL}\right)^{-1} \quad (17)$$

and

$$G_{LT,m} = G_{LT} \exp\left(-1.64V_{GLT} - 0.5V_{GLT}\right)^{-1}. \quad (18)$$

Reported in Table 3 are the seven basic variables in Eq. (15). Column (1) gives the beam labelling in the form of section type (I or C1), followed, after the hyphen, with beam span L (e.g. 1828 mm). Columns (2) to (5) list the measured section properties of I_T, I_w, I_z and W_y. It is observed that their CVs for the I-shape are in the range of 0.36 to 1.2% and similar for the C1-shape at 0.76 to 1.29%. For an PFRP I-section Trumpf [21] determined CVs for the same geometrical properties in range of 0.79% to 1.81%. In reference [34] for the calibration of steel sections these four section properties have a specified CV, which is slightly higher at 3%.

By substituting the test results from Table 1 into Eqs. (17) and (18) the population means of $E_{L,m}$ and $G_{LT,m}$ were determined, and they are reported in Table 3. Except for the basic variable G_{LT} having a CV of 8% for the I-shape the other basic variables for both shapes have CVs below 4%.

Step 2: *Compare test results (r_e) and theoretical predictions (r_t)*

The theoretical moment of resistances $r_{t,i}$ (i = 1 to n, where n is number of test results) are obtained by substituting the mean variables listed in columns (2) to (8) of Table 3 into the resistance function of Eq. (15). To calculate M_{cr} using Eq. (8) to obtain χ_{LT} by Eq. (15) and Eq.(10), the terms C_1 and C_2 are for moment distribution, z_g for loading height and k for displacement boundary conditions and k_w is assumed to be 1.0. The 114 beam configurations failing with the LTB mode [4] were loaded in three-point bending

with simply supported ends. When calculating M_{cr} the justification for C_1 = 1.344 and C_2 = 0.630 with $k = k_w$ = 1.0 and C_1 = 1.107 and C_2 = 0.432 with k = 0.5 and k_w = 1.0 is given in Section 4.7 of [4].

The experimental moment resistances, $r_{e.i}$, are determined using:

$$r_{e,i} = \frac{P_{cr,e,i} \times L}{4} \tag{19}$$

In Eq. (19) $P_{cr,e,i}$ is for the experimental LTB point loads reported in [4] (and [5]) for a beam of a single shape (I or C1) having span L and loaded in three-point bending for flexure about the major y-y axis. The variables in a LTB test series are five spans, the two displacement end boundary conditions of EC1 (with k = 1.0 for simply supported for flexure about minor axis) and EC2 (with k = 0.5 for clamped supported for flexure about minor axis) and the three vertical load heights of SC (z_g = 0 mm), Top Flange (TF for $z_g = +h/2$) and Bottom Flange (BT for $z_g = -h/2$). h is the depth of the PFRP section.

Column (1) in Table 4 is for the labelling [4] of 10 I-beam configurations. In columns (2) and (3) are the $10r_e$ and $10r_t$ results for TF loading that has the lowest elastic critical resistance moment. Equivalent results for the SC loading case are reported in columns (4) and (5) and those for the BF situation, giving the highest resistance moment, in columns (6) and (7). The equivalent $30r_e$ and $30r_t$ values for the 10 C1-beam configurations are reported in Table 5.

Figures 7 and 8 are plots of r_e vs. r_t created from the data given in Tables 4 and 5. In the figures the points for boundary condition EC1 (for $k = k_w$ = 1.0 in Eq. (8)) are given by the circular shaped symbol and those for EC2 (for k = 0.5 and k_w = 1.0) have a rectangular symbol. A linear solid line for $r_e = r_t$ is introduced to highlight that, had the 'design model' been exact and complete, every point would exactly lie on this line. As

is normally found with real data there is a degree of scatter in Figures 7 and 8 and r_e (measured) is generally higher than r_t (theoretical).

Step 3: *Calculate the mean correction factor* b_m

The mean correction factor, b_m, can be estimated using:

$$b_m = \frac{\sum r_e r_t}{\sum r_t^2} \tag{20}$$

with the summation over the *n* tests for a particular beam cross-section shape. Results in Tables 4 and 5 give b_m = 1.29 for the I-beams and 1.27 for the C1-beams. Figures 9 and 10 are for plots of ratio r_e/r_t against $\bar{\lambda}_{LT}$ for 30 tested beams of the two shapes. It is seen that with the I-beams all the points lie above the horizontal line r_e/r_t = 1, which means the expression for r_t is giving 'safe' predictions. Results from the tested C1-beams give a higher scatter, especially with the EC2 displacement boundary conditions, which gives a single point below the line r_e/r_t = 1.

Step 4: *Determination of the CV for the error terms*

Error term δ_i $(i = 1 \rightarrow n)$ for each test result, $r_{e,i}$, is calculated from:

$$\delta_i = \frac{r_{e,i}}{b_m r_{t,i}} \tag{21}$$

Estimation for the CV for the error term, V_δ, is obtained from:

$$V_\delta = \sqrt{\exp\left(s_\Delta^2\right) - 1} \tag{22}$$

where

$$s_\Delta^2 = \frac{1}{n-1}\sum_{i=1}^{n}\left(\Delta_i - \bar{\Delta}\right)^2 \tag{23}$$

In Eq. (23), $\Delta_i = \ln(\delta_i)$ and $\bar{\Delta} = \frac{1}{n}\sum_{i=1}^{n}\Delta_i$.

Reported in Tables 6 and 7 are the error terms of δ_i and Δ_i for the two shapes. These two parameters for 10 different beam configurations are presented in columns (2) and (3) for TF loading, in columns (4) and (5) for SC and in clumns (6) and (7) for BF loading. V_δ is calculated on introducing the 30 tabulated error terms into Eqs. (23) and (22) and is found to be 0.101 for the I-beams and 0.112 for the C1-beams, which are both close to 10%.

Step 5: *Examine the compatibility*

The purpose of the fifth step is to examine the compatibility of the test results with the assumptions in the 'design model'. It is suggested that if the scatter of the $r_{e,i}$ and $r_{t,i}$ pairs by engineering judgement is too high, it can be lowered by either adjusting the design model to accounts for the 'ignored' variables or to separate the test results into sub-groups, in which the contribution of the missing variables can be considered constant. In this investigation, all of the influencing factors have been adequately taken into consideration. It is found that the r_e-r_t pairs for the I-beams spread evenly and so the scatter is not too high. There are data pairs from the C1 tests that do, however, present a larger scatter. In this preliminary study it was decided not to alter the design model for the calibration of γ_M.

Step 6: *Calculate the coefficients of variation for the basic parameters*

The CVs (V_{Xi}) for the seven basic parameters in the resistance function Eq. (15) are presented in Table 3. For the I-shape they are listed in the eighth row and in the sixteenth row for the C1 shape.

Step 7: *Determine the characteristic value of the resistance* r_k

To determine the characteristic resistance, r_k, it is required that the CV for V_r be calculated from:

$$V_r = \sqrt{V_\delta^2 + V_{rt}^2}\,. \tag{24}$$

V_{rt} should be calculated using:

$$V_{rt} = \frac{1}{g_{rt}^2\left(\underline{X}_m\right)} \times \sum_{i=1}^{j}\left(\frac{\partial g_{rt}}{\partial X_i}\sigma_i\right)^2 \tag{25}$$

where $g_{rt}(\underline{X}_m)$ is obtained from Eq. (15), j is the number of basic parameters, $\underline{X}_m$ is the mean of the basic parameters and σ_i is the Standard Deviation (SD) of each basic parameter, as reported in Table 3.

Eq. (25) is computed using Matlab [35] for the V_{rt}s listed in column (2) of Tables 8 and 9. In column (1) are the label's for the 30 different beam configurations in the programme of LTB tests [4] and [5]. It is seen in Table 9 that these CVs are very small, having a maximum of ≅ 0.003 for the I-beams in Table 8 and ≅ 0.007 for the C1-beams. When substituting V_δ and V_{rt} into Eq. (24) for V_r, the contribution of V_{rt} can be ignored for the I-shape since:

$$V_r = \sqrt{V_\delta^2 + V_{rt}^2} = \sqrt{0.101^2 + 0.003^2} = 0.10105 \cong 0.101 = V_\delta\,.$$

Similarly, for the C1-shape we have:

$$V_r = \sqrt{V_\delta^2 + V_{rt}^2} = \sqrt{0.112^2 + 0.007^2} = 0.1122 \cong 0.112 = V_\delta$$

It is acceptable in the calibration procedure to treat $V_r = V_\delta$. A similar observation is given by Trumpf [21], who, when calibrating the design model for the LTB mode of failure, found the contribution from V_{rt} small enough to be ignored.

The process requires that, when the number of individual tests is limited (i.e. $n < 100$), r_k should be determined by:

$$r_k = b_m g_{rt}(\underline{X}_m)\exp(-k_\infty \alpha_{rt} Q_{rt} - k_n \alpha_\delta Q_\delta - 0.5Q^2) \tag{26}$$

with:

$$Q_{rt} = \sigma_{\ln(rt)} = \sqrt{\ln(V_{rt}^2 + 1)} = V_{rt} \tag{27}$$

$$Q_\delta = \sigma_{\ln(\delta)} = \sqrt{\ln(V_\delta^2 + 1)} \tag{28}$$

$$Q = \sigma_{\ln(r)} = \sqrt{\ln(V_r^2 + 1)} = Q_\delta \tag{29}$$

$$\alpha_{rt} = \frac{Q_{rt}}{Q} \tag{30}$$

$$\alpha_\delta = \frac{Q_\delta}{Q} = 1 \tag{31}$$

In Eq. (26) k_n is the characteristic fractile factor from Table D1 on page 79 of BS EN 1990:2002 [30] for "V_X unknown"; V_X is Eurocode notation for CV. For the calibration of γ_M we have n = 30 and k_n is 1.73. When n tends to ∞ we have the limiting k_n, which is k_∞ = 1.64.

In columns (2) to (5) of Tables 8 and 9 are the values for Q_{rt}, $Q_\delta = Q$, α_{rt} and r_k obtained using Eqs. (26) to (31).

Steps 1 to 7 are explicitly found in EN 1990:2002, whilst Steps 8 and 9 to complete the calibration procedure for γ_M are not assigned numbers.

Step 8: *Obtain the design value of the resistance,* r_d

The design value of the resistance, r_d, for the test population that has < 100 test results should be calculated using:

$$r_d = b_m g_{rt}(\underline{X}_m)\exp(-k_{d,\infty}\alpha_{rt}Q_{rt} - k_{d,n}\alpha_\delta Q_\delta - 0.5Q^2) \tag{32}$$

In Eq. (32), the variable $k_{d,n}$ is the design fractile factor from Table D2 on page 79 in BS EN 1990:2002 [30] for "V_X unknown". In this study, $k_{d,n}$ is 3.13 for n = 30. Note $k_{d,\infty}$ is the value for n tends to ∞, and from Table D2 is 3.04.

Step 9: *Determine the safety partial factor* γ_M

γ_M, which accounts for material property and for model uncertainties and dimensional variations, can be determined from:

$$\gamma_M = \frac{r_k}{r_d} \tag{33}$$

Columns (6) and (7) in Tables 8 and 9 present r_d from Eq. (32) and γ_M by Eq. (33). To three significant figures it is found that γ_M for LTB failure lies in the narrow ranges of 1.14 to 1.18 for the I-shape and 1.16 to 1.19 for the C1-shape. Taking into account the degree of uncertainties in the seven basic variables (Table 3), and to provide for a higher reliability in design, the authors propose, for PFRP beams in bending that γ_M be taken as 1.3 (for the LTB mode of failure at ultimate limit state).

4.4 Lateral-torsional buckling curves

Plotted as thick dashed lines in Figs. 11 and 12 are the specific LTB curves of χ_{LT} (≤ 1.0) against λ_{LT} (0 to 4.0) for the I and C1 shapes, having α_{LT} =0.34 and γ_M = 1.3. In the

two figures the solid line is the unfactored LTB curve with the χ_{LT} axis on the left-side. χ_{LT} for the factored situation is given on the right side. It is noted that, when an LTB curve is presented in a design standard, the dashed line curve would not exist. It is observed from the results given in Figs. 11 and 12 that all 30 test results for LTB failure are positioned above the factored curve. This finding ensures the design procedure is going to be safe and reliable. The results presented in these two figures provide strong evidence that an imperfection factor α_{LT} = 0.34 and partial factor γ_M = 1.3 would be appropriate for the two shapes in the calibration study.

For a comparison with an independent calibration, it is noteworthy that in the American pre-standard for PFRP standard shapes [8] the resistance factor, ϕ, for the LTB mode of failure is 0.7. This is equivalent to γ_M = 1.43 from $\gamma_M \cong 1/\phi$. Trumpf applied the same Eurocode approach (EN 1990:2002) in 2006 [21] in his LTB study with PFRP I-shapes to established a mean γ_{M1} ($\cong\gamma_M$) of 1.41. Finding that 1.43 and 1.41 are the same, and higher than 1.3, it can be proposed that the test results and calibration assumptions used by the authors are more reliable than those available, in 2010, when ϕ was determined using the approach developed in [36].

To construct the generic LTB curve (with γ_M = 1.3) presented in Fig. 13 the authors combined 114 LTB test results. By making the assumption that $\sigma_{Loc} = 134$ MPa is for the ultimate failure stress that establishes χ_{LT} =1.0, design parameters $\bar{\lambda}_{LT}$ and χ_{LT} for the beam configurations of I, C1 to C3 shapes were calculated. The results in the Fig. 13 plot provide us with further evidence that the proposed design procedure can be reliable.

5. CONCLUSIONS

A proposed design procedure to determine the resistance of pultruded FRP thin-walled members in bending failing with the Ultimate Limit State (ULS) mode of Lateral-Torsional Buckling (LTB) has been formulated based on the Eurocode 3 approach for steel sections. Recommended is a plateau length for the LTB curve ($\bar{\lambda}_{LT,0}$) of 0.5 and an imperfection factor (α_{LT}) of 0.34. The calibration procedure for the partial factor γ_M ($\cong \gamma_{M1}$) follows the steps in Annex D of EN 1990:2002. It is shown that for this specific ULS mode of failue that the partial factor for members of an I-shape lies is in the narrow range of 1.14 to 1.18 and for a C-shape it is from 1.16 to 1.19. To take account of the level of uncertainty in the measured geometries and failure load results, and in the underlying assumptions made, a γ_M of 1.3 for PFRP members in bending is proposed. By incorporating the 114 test results into a single LTB curve with this partial factor of resistance and by assuming a local flange buckling strength is 134 MPa for the four shapes tested it is observed that the LTB curve could be for generic design.

It is noteworthy that in an American Society of Civil Engineering pre-standard for the design of PFRP structures the resistance factor (ϕ) for LTB failure is 0.7, which is equivalent to γ_M of 1.4. The fact that 1.4 is higher than our recommended partial factor of 1.3 shows that the LTB test results and calibration process used in this paper are likely to be more reliable than those available in 2010 when the pre-standard ϕ was determined.

ACKNOWLEDGEMENTS

The authors gratefully acknowledge Dr. Heiko Trumpf (Bollinger and Grohmann, Germany) for his comments and suggestions that were important to the preparation of this paper. The first author gratefully acknowledges his scholarships from the Vietnamese International Education Development (VIED) and the School of Engineering at The University of Warwick, UK.

REFERENCES

1. Bank LC. Composites for construction: Structural design with FRP materials. 2006, NJ, USA: John Willey & Sons.

2. Mottram JT. Does performance based design with fibre reinforced polymer components and structures provide any new benefits and challenges. The Structural Engineer 2011;89**(**6):23-27.

3. Gand AK, Chan TM, Mottram JT. Civil and structural engineering applications, recent trends, research and developments on pultruded fiber reinforced polymer closed sections: a review. Front Structural Civil Eng 2013;7(3):227–244.

4. Nguyen TT. Lateral-torsional buckling resistance of pultruded fibre reinforced polymer shapes. 2014, University of Warwick.

5. Nguyen TT, Chan TM, Mottram JT. Lateral-torsional buckling resistance by testing for pultruded FRP beams under different loading and displacement boundary conditions. Composites Part B: Engineering 2014;60:306-318.

6. Mottram JT. Lateral-torsional buckling of a pultruded I-beam. Composites 1992;23(2):81-92.

7. AISC, Specification for Structural Steel Buildings, in ANSI/AISC 360. 2010, American Institute of Steel Construction: Chicago, IL, USA.

8. ASCE, Pre-standard for load and resistance factor design (LRFD) of pultruded fiber reinforced polymer (FRP) structures. 2010: Arlington, VA,USA.

9. BSI, Eurocode 3: Design of Steel Structures - Part 1-1: General Rules and Rules for Buildings, in BS EN 1993-1-1. 2005, British Standards Institution: London, UK.

10. Szalai J, Papp F. On the theoretical background of the generalization of Ayrton–Perry type resistance formulas. Journal of Constructional Steel Research 2010;66(5):670-679.

11. Gutiérrez E, Dimova S, Pinto A. Purpose and justification for new design standards regarding the use of fibre-reinforced polymer composites in civil engineering. EUR 22864 EN-2007, Joint Research Centre, European Commission, 2007.

12. Timoshenko S. Theory of elastic stability. 1936, New York: McGraw-Hill

13. Flint AR. On the lateral stability of beams, in Engineering. 1948, University of Bristol.

14. Clark JW, Hill HN. Lateral Buckling of Beams. Journal of the Structural Division-ASCE 1960;86(ST7):175-196.

15. Trahair NS. Flexural-torsional buckling of structures. 1993, London, UK: CRC Press.

16. Bureau A. NCCI: Elastic critical moment for lateral torsional buckling, in SN003a-EN-EU. 2006, Access Steel

17. BSI, Eurocode 3: design of steel structures, Part 1.1 General rules for buildings, in DD ENV 1993-1-1. 1992, British Standards Institution: London, UK.

18. Kollár LP, Springer GS. Mechanics of composite structures. 2003, Cambridge: University press.

19. Allen HG, Bulson PS. Background to buckling. 1980, London: McGraw-Hill.

20. Razzaq Z, Prabhakaran R, Sirjani MM. Load and resistance factor design (LRFD) approach for reinforced-plastic channel beam buckling. Composites Part B: Engineering 1996;27(3):361-369.

21. Trumpf H. Local and global stability of plane frame works made of orthotropic FRP profiles. PhD Thesis, 2006, University of Aachen, Germany: Shaker-Verlag. (in German)

22. BSI, Plastics - Determination of tensile properties - Part 1: General principles, in BS EN ISO 527-1. 2012, British Standards Institution: London, UK.

23. BSI, Plastics - Determination of tensile properties - Part 4: Test conditions for isotropic and orthotropic fibre-reinforced plastic composites, in BS EN ISO 527-4. 1997, British Standards Institution: London, UK.

24. ASTM, Standard test method for shear properties of composite materials by the V-notched beam method, in D5379 / D5379M. 2012, ASTM International: West Conshohocken, PA, USA.

25. ASTM, Standard test method for shear properties of composite materials by V-notched rail shear method, in D7078 / D7078M. 2012, ASTM International: West Conshohocken, PA, USA.

26. BSI, Reinforced plastics - Determination of the in-plane shear modulus by the plate twist method, in BS EN 15310. 2005, British Standards Institution: London, UK.

27. Hodgkinson J. Mechanical testing of advanced fibre composites. 2000, Cambridge, UK: Woodhead Publishing Limited.

28. Chamis CC, Sinclair JH. Ten-deg off-axis test for shear properties in fiber composites. Experimental Mechanics 1977;17(9):339-346.

29. BSI, Plastics - Determination of tensile properties - Part 5: Test conditions for unidirectional fibre-reinforced plastic composites, in BS EN ISO 527-5. 2009, British Standards Institution: London, UK.

30. BSI, Eurocode. Basis of structural design, in BS EN 1990. 2002, British Standards Institution: London, UK.

31. Kollár LP. Local buckling of fiber reinforced plastic composite structural members with open and closed cross sections. J Struct Eng 2003;129(11):1503-1513.

32. Mottram JT. Determination of critical load for flange buckling in concentrically loaded pultruded columns. Compos Part B: Engng 2004;35(1):35-47.

33. IES Inc, ShapeBuilder Ver 7.0. 2013: Bozeman, MT, US.

34. Sedlacek G, Ungermann D, Kuck J, Maquoi R, Janss J. 'Eurocode 3 – Part 1.1, Design of Steel Structures: General Rules and Rules for Buildings, Background documentation. Chapter 5.03, Evaluation of test results with cross-sectional classes 1-3 in order to obtain strength functions and suitable model factors,' Oct.1989.

35. Mathworks Inc, MATLAB 2013: Natick, Massachusetts, Unite States.

36. Zureick A-H, Bennett RM, Ellingwood BR. Statistical characterization of FRP composite material properties for structural design. J Struct Engrg. 2006; 132(8):1320-1327.

Figure captions

Table

Table 1

Elastic constants and the corresponding statistical data.

[1]Section	[2]E_L (GPa)	[3]CV (%)	[4]SD (GPa)	[5]G_{LT} (GPa)	[6]CV (%)	[7]SD (GPa)
I	30.6	2.3	0.70	4.2	8.1	0.34
C1	31.6	3.5	1.10	4.8	3.0	0.14
C2	32.9	1.9	0.60	4.8	4.2	0.20
C3	29.2	3.9	1.10	4.2	8.6	0.36

Table 2

Generalized imperfection factor η_{LT}.

[1]Specimen	[2]v_0 (mm)	[3]φ_0 (rad)	[4]W_y (mm^3)	[5]W_w (mm^4)	[6]W_z (mm^3)	[7]M_{cr} (kN.m)	[8]η_{LT}	[9]α_{LT}
I-1828	0.78	0.013	4.65×10^4	3.92×10^5	3.63×10^3	1.62×10^6	0.18	0.11
I-2438	2.86	0.036				1.08×10^6	0.51	0.26
I-2844	1.95	0.021				8.87×10^5	0.31	0.14
I-3454	2.72	0.024				6.98×10^5	0.36	0.14
C1-1828	0.27	0.006	4.30×10^4	3.30×10^5	4.63×10^3	1.37×10^6	0.05	0.04
C1-2438	0.80	0.013				1.02×10^6	0.11	0.07
C1-2844	1.55	0.021				8.78×10^5	0.18	0.11
C1-3454	1.72	0.019				7.23×10^5	0.16	0.08

Table 3

Basic variables and their statistical data.

[1]Specimen	[2]I_T (mm^4)	[3]I_w (mm^6)	[4]I_z (mm^4)	[5]W_y (mm^3)	[6]E_L (N/mm^2)	[7]G_{LT} (N/mm^2)	[8]σ_{Loc} (N/mm^2)
I-1828	1.71×10^4	7.03×10^8	2.18×10^5	4.95×10^4	30600	4200	134
I-2438	1.68×10^4	7.00×10^8	2.17×10^5	4.97×10^4			
I-2844	1.73×10^4	7.05×10^8	2.19×10^5	4.99×10^4			
I-3454	1.72×10^4	7.06×10^8	2.19×10^5	4.95×10^4			
I-4064	1.68×10^4	6.99×10^8	2.16×10^5	4.97×10^4			
Mean	*1.70×10^4*	*7.03×10^8*	*2.18×10^5*	*4.97×10^4*	*32000*	*5000*	*166*
SD	*210*	*3.21×10^6*	*1.14×10^3*	*180*	*700*	*340*	*13.4*
CV (%)	*1.2*	*0.46*	*0.53*	*0.36*	*2.17*	*8.09*	*10*
C1-1828	1.52×10^4	6.46×10^8	2.83×10^5	4.43×10^4	31600	4800	100
C1-2438	1.52×10^4	6.36×10^8	2.74×10^5	4.27×10^4			
C1-2844	1.49×10^4	6.34×10^8	2.78×10^5	4.38×10^4			
C1-3454	1.52×10^4	6.43×10^8	2.76×10^5	4.27×10^4			
C1-4064	1.52×10^4	6.37×10^8	2.77×10^5	4.31×10^4			
Mean	*1.51×10^4*	*6.39×10^8*	*2.78×10^5*	*4.32×10^4*	*34060*	*5100*	*124*
SD	*140*	*4.48×10^6*	*3.58×10^3*	*530*	*1100*	*140*	*10.0*
CV (%)	*0.91*	*0.76*	*1.29*	*1.24*	*3.50*	*2.91*	*10*

Table 4

r_e and r_t for the I-section.

[1]Specimen	TF (Top Flange)		SC (Shear Centre)		BF (Bottom Flange)	
	[2] r_e (kN.m)	[3] r_t (kN.m)	[4] r_e (kN.m)	[5] r_t (kN.m)	[6] r_e (kN.m)	[7] r_t (kN.m)
I-1828_EC1	1.73	1.23	2.80	1.85	4.17	2.71
I-2438_EC1	1.26	0.89	1.77	1.27	2.40	1.79
I-2844_EC1	1.17	0.78	1.49	1.07	1.84	1.46
I-3454_EC1	0.93	0.65	1.11	0.85	1.39	1.12
I-4064_EC1	0.73	0.55	0.91	0.70	1.13	0.89
I-1828_EC2	2.87	1.87	-	3.18	-	4.82
I-2438_EC2	2.03	1.32	2.76	2.14	3.68	3.34
I-2844_EC2	1.49	1.15	2.30	1.78	3.19	2.71
I-3454_EC2	1.27	0.95	1.74	1.40	2.27	2.04
I-4064_EC2	1.05	0.81	1.36	1.14	1.71	1.60

Table 5

r_e and r_t for the C1-section.

[1]Specimen	TF (Top Flange)		SC (Shear Centre)		BF (Bottom Flange)	
	[2] r_e (kN.m)	[3] r_t (kN.m)	[4] r_e (kN.m)	[5] r_t (kN.m)	[6] r_e (kN.m)	[7] r_t (kN.m)
C1-1828_EC1	1.51	1.27	2.53	1.96	3.46	2.84
C1-2438_EC1	1.11	0.94	1.85	1.37	2.58	1.97
C1-2844_EC1	1.03	0.81	1.39	1.16	1.88	1.63
C1-3454_EC1	0.86	0.69	1.29	0.93	1.52	1.26
C1-4064_EC1	0.66	0.60	0.81	0.79	1.13	1.03
C1-1828_EC2	2.29	1.84	3.86	3.06	5.80	3.99
C1-2438_EC2	2.00	1.34	3.00	2.21	4.46	3.23
C1-2844_EC2	1.33	1.16	2.48	1.88	3.05	2.82
C1-3454_EC2	1.26	0.99	1.74	1.50	-	2.21
C1-4064_EC2	1.03	0.87	1.28	1.26	1.62	1.80

Table 6

δ_i and Δ_i for I-section.

[1]Specimen	TF (Top Flange)		SC (Shear centre)		BF (Bottom Flange)	
	[2] δ_i	[3] Δ_i	[4] δ_i	[5] Δ_i	[6] δ_i	[7] Δ_i
I-1828_EC1	1.08	-0.081	1.17	-0.157	1.19	-0.172
I-2438_EC1	1.09	-0.089	1.08	-0.074	1.04	-0.036
I-2844_EC1	1.16	-0.148	1.08	-0.072	0.97	0.026
I-3454_EC1	1.12	-0.111	1.01	-0.011	0.96	0.042
I-4064_EC1	1.03	-0.031	1.01	-0.009	0.98	0.025
I-1828_EC2	1.19	-0.170	-	-	-	-
I-2438_EC2	1.19	-0.171	1.00	0.004	0.85	0.160
I-2844_EC1	1.01	-0.005	1.00	0.001	0.91	0.094
I-3454_EC2	1.03	-0.030	0.96	0.044	0.86	0.150
I-4064_EC2	1.00	0.004	0.92	0.083	0.82	0.193

Table 7

δ_i and Δ_i for C1-section.

[1]Beam	TF (Top Flange)		SC (Shear centre)		BF (Bottom Flange)	
	[2] δ_i	[3] Δ_i	[4] δ_i	[5] Δ_i	[6] δ_i	[7] Δ_i
C1-1828_EC1	0.94	0.065	1.01	-0.013	0.96	0.045
C1-2438_EC1	0.93	0.070	1.06	-0.055	1.03	-0.029
C1-2844_EC1	1.00	-0.001	0.95	0.056	0.91	0.098
C1-3454_EC1	0.99	0.010	1.08	-0.080	0.95	0.054
C1-4064_EC1	0.87	0.140	0.81	0.206	0.86	0.148
C1-1828_EC2	0.98	0.022	0.99	0.010	1.14	-0.133
C1-2438_EC2	1.17	-0.157	1.06	-0.063	1.09	-0.082
C1-2844_EC2	0.90	0.106	1.04	-0.039	0.85	0.162
C1-3454_EC2	1.00	-0.002	0.91	0.098	-	-
C1-4064_EC2	0.93	0.072	0.80	0.226	0.70	0.350

Table 8

Calculation of partial factor γ_M for I-section.

[1]Specimen	[2]$Q_{rt} = V_{rt}$	[3]$Q_\delta = Q$	[4]α_{rt}	[5]r_k	[6]r_d	[7]γ_M
I-1828_TF_EC1	0.0010		0.0095	1.41	1.22	1.156
I-1828_SC_EC1	0.0007		0.0066	2.08	1.81	1.149
I-1828_BF_EC1	0.0006		0.0057	3.05	2.64	1.155
I-2438_TF_EC1	0.0012		0.0121	1.04	0.90	1.156
I-2438_SC_EC1	0.0008		0.0080	1.45	1.26	1.151
I-2438_BF_EC1	0.0006		0.0056	2.02	1.75	1.154
I-2844_TF_EC1	0.0014		0.0140	0.89	0.77	1.156
I-2844_SC_EC1	0.0009		0.0093	1.21	1.05	1.152
I-2844_BF_EC1	0.0006		0.0063	1.63	1.41	1.156
I-3454_TF_EC1	0.0015		0.0153	0.74	0.64	1.156
I-3454_SC_EC1	0.0011		0.0105	0.96	0.84	1.143
I-3454_BF_EC1	0.0007		0.0071	1.26	1.09	1.156
I-4064_TF_EC1	0.0016		0.0156	0.65	0.55	1.182
I-4064_SC_EC1	0.0011		0.0110	0.81	0.70	1.157
I-4064_BF_EC1	0.0008	0.101	0.0076	1.02	0.88	1.159
I-1828_TF_EC2	0.0009		0.0091	2.15	1.85	1.162
I-1828_SC_EC2	0.0008		0.0075	3.63	3.14	1.156
I-1828_BF_EC2	0.0026		0.0259	5.64	4.88	1.156
I-2438_TF_EC2	0.0013		0.0125	1.54	1.33	1.158
I-2438_SC_EC2	0.0008		0.0075	2.46	2.13	1.155
I-2438_BF_EC2	0.0007		0.0074	3.81	3.30	1.155
I-2844_TF_EC2	0.0015		0.0149	1.32	1.14	1.158
I-2844_SC_EC2	0.0009		0.0088	2.02	1.75	1.154
I-2844_BF_EC2	0.0006		0.0061	3.03	2.63	1.152
I-3454_TF_EC2	0.0017		0.0166	1.10	0.95	1.158
I-3454_SC_EC2	0.0010		0.0101	1.60	1.38	1.159
I-3454_BF_EC2	0.0006		0.0062	2.29	1.98	1.157
I-4064_TF_EC2	0.0017		0.0170	0.95	0.83	1.145
I-4064_SC_EC2	0.0011		0.0107	1.32	1.14	1.158
I-4064_BF_EC2	0.0007		0.0066	1.82	1.58	1.152

Table 9

Calculation of partial factor γ_M for C1-section.

[1]Specimen	[2]$Q_{rt} = V_{rt}$	[3]$Q_\delta = Q$	[4]α_{rt}	[5]r_k	[6]r_d	[7]γ_M
C1-1828_TF_EC1	0.0006		0.0055	1.35	1.16	1.164
C1-1828_SC_EC1	0.0008		0.0074	2.11	1.81	1.166
C1-1828_BF_EC1	0.0023		0.0206	3.13	2.68	1.168
C1-2438_TF_EC1	0.0006		0.0049	1.01	0.86	1.174
C1-2438_SC_EC1	0.0007		0.0060	1.49	1.28	1.164
C1-2438_BF_EC1	0.0009		0.0082	2.17	1.86	1.167
C1-2844_TF_EC1	0.0005		0.0048	0.87	0.75	1.160
C1-2844_SC_EC1	0.0006		0.0058	1.25	1.07	1.168
C1-2844_BF_EC1	0.0009		0.0076	1.77	1.51	1.172
C1-3454_TF_EC1	0.0005		0.0048	0.73	0.63	1.159
C1-3454_SC_EC1	0.0006		0.0055	1.00	0.86	1.163
C1-3454_BF_EC1	0.0008		0.0069	1.37	1.17	1.171
C1-4064_TF_EC1	0.0005		0.0048	0.64	0.54	1.185
C1-4064_SC_EC1	0.0006		0.0053	0.84	0.72	1.167
C1-4064_BF_EC1	0.0007	0.112	0.0065	1.11	0.95	1.168
C1-1828_TF_EC2	0.0007		0.0060	1.98	1.69	1.172
C1-1828_SC_EC2	0.0034		0.0303	3.41	2.91	1.172
C1-1828_BF_EC2	0.0069		0.0615	4.67	3.99	1.170
C1-2438_TF_EC2	0.0006		0.0050	1.45	1.24	1.169
C1-2438_SC_EC2	0.0009		0.0078	2.45	2.09	1.172
C1-2438_BF_EC2	0.0047		0.0421	3.72	3.18	1.170
C1-2844_TF_EC2	0.0005		0.0048	1.26	1.07	1.178
C1-2844_SC_EC2	0.0007		0.0064	2.04	1.74	1.172
C1-2844_BF_EC2	0.0021		0.0190	3.13	2.68	1.168
C1-3454_TF_EC2	0.0005		0.0049	1.06	0.91	1.165
C1-3454_SC_EC2	0.0006		0.0058	1.63	1.39	1.173
C1-3454_BF_EC2	0.0010		0.0090	2.44	2.09	1.167
C1-4064_TF_EC2	0.0005		0.0048	0.93	0.79	1.177
C1-4064_SC_EC2	0.0006		0.0055	1.36	1.16	1.172
C1-4064_BF_EC2	0.0008		0.0075	1.96	1.68	1.167

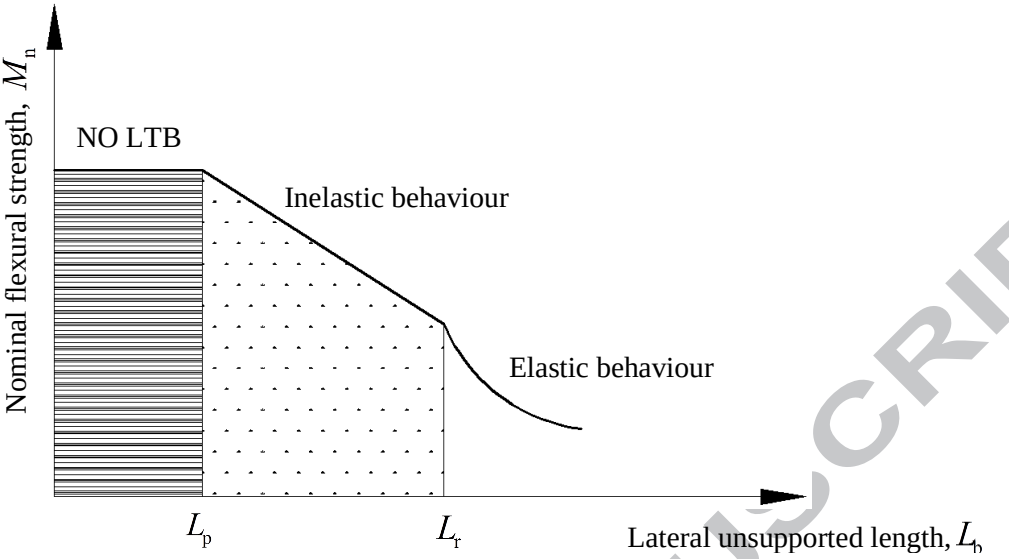
Nominal flexural strength, M_n
NO LTB
Inelastic behaviour
Elastic behaviour
L_p
L_r
Lateral unsupported length, L_b

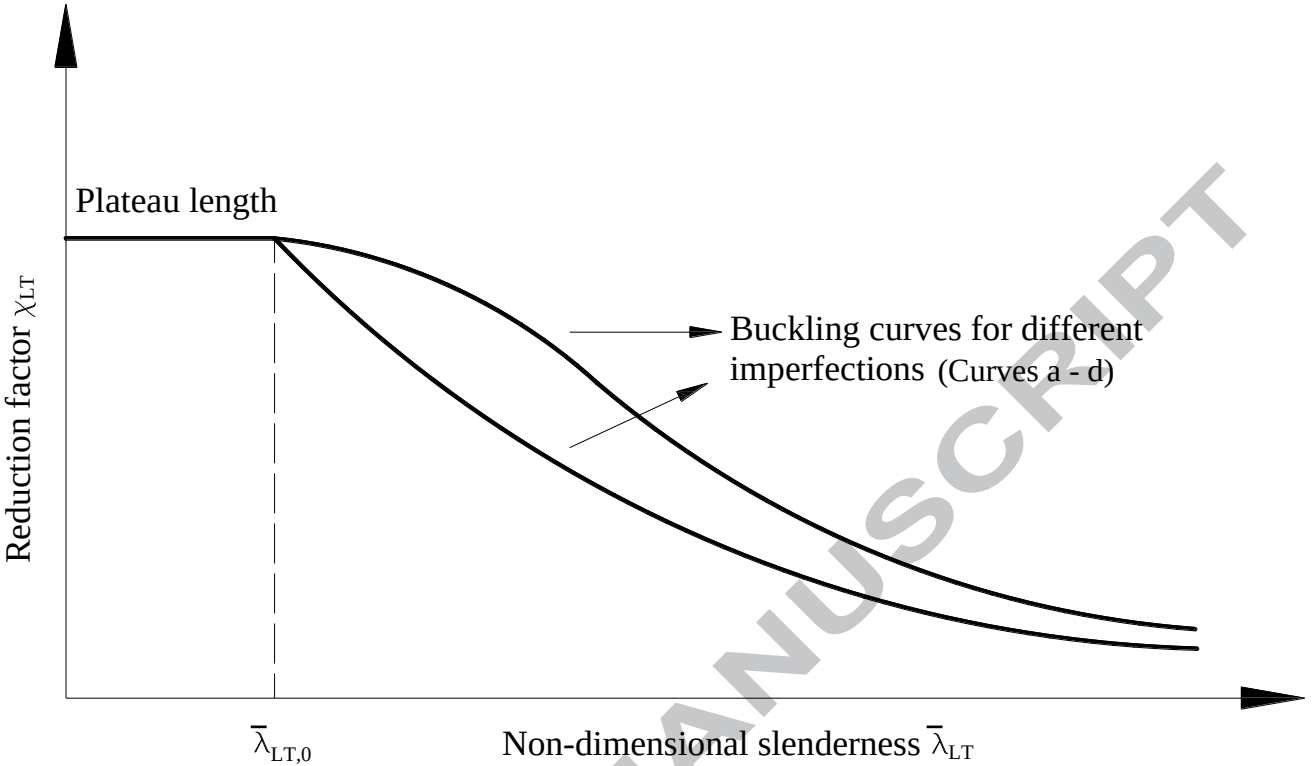
Plateau length
Reduction factor χ_{LT}
Buckling curves for different imperfections (Curves a - d)
$\bar{\lambda}_{LT,0}$
Non-dimensional slenderness $\bar{\lambda}_{LT}$

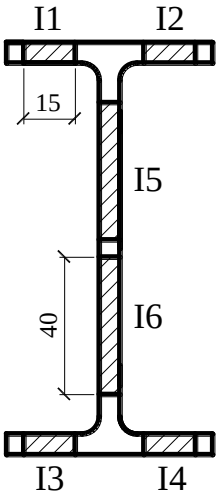

I section
(120 ×60 ×6 mm)

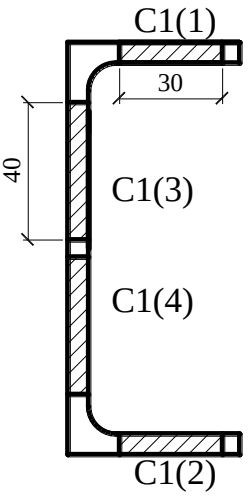

C1 section
(120 ×50 ×6 mm)

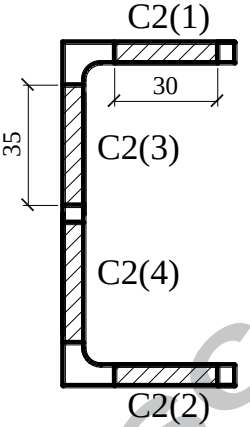

C2 section
(100 ×50 ×6 mm)

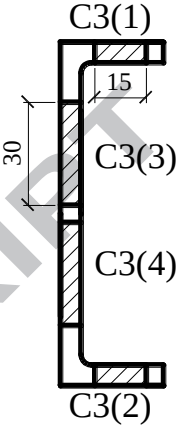

C3 section
(100 ×30 ×6 mm)

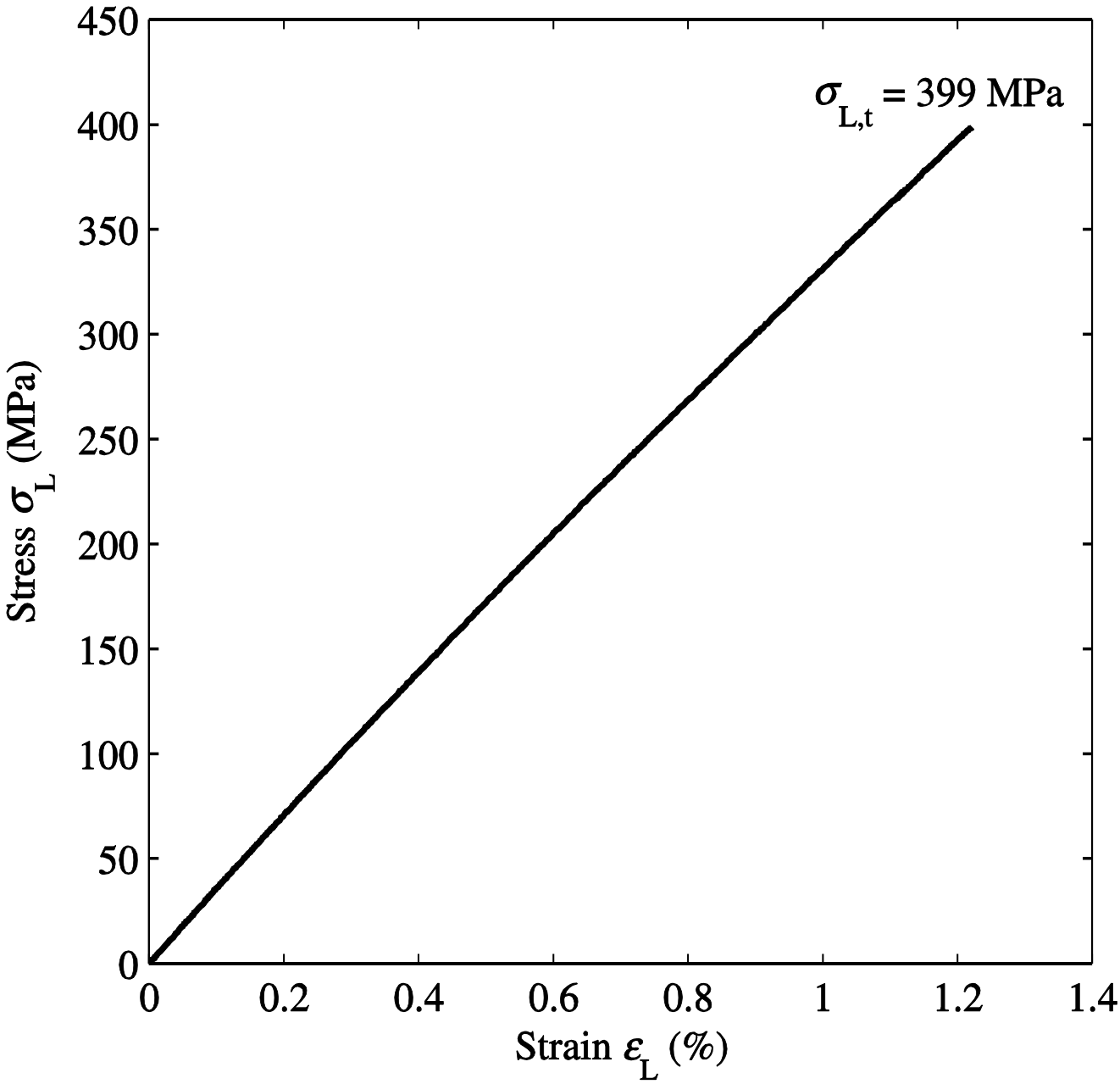
$\sigma_{L,t}$ = 399 MPa
Stress σ_L (MPa)
Strain ε_L (%)
450
400
350
300
250
200
150
100
50
0
0
0.2
0.4
0.6
0.8
1
1.2
1.4

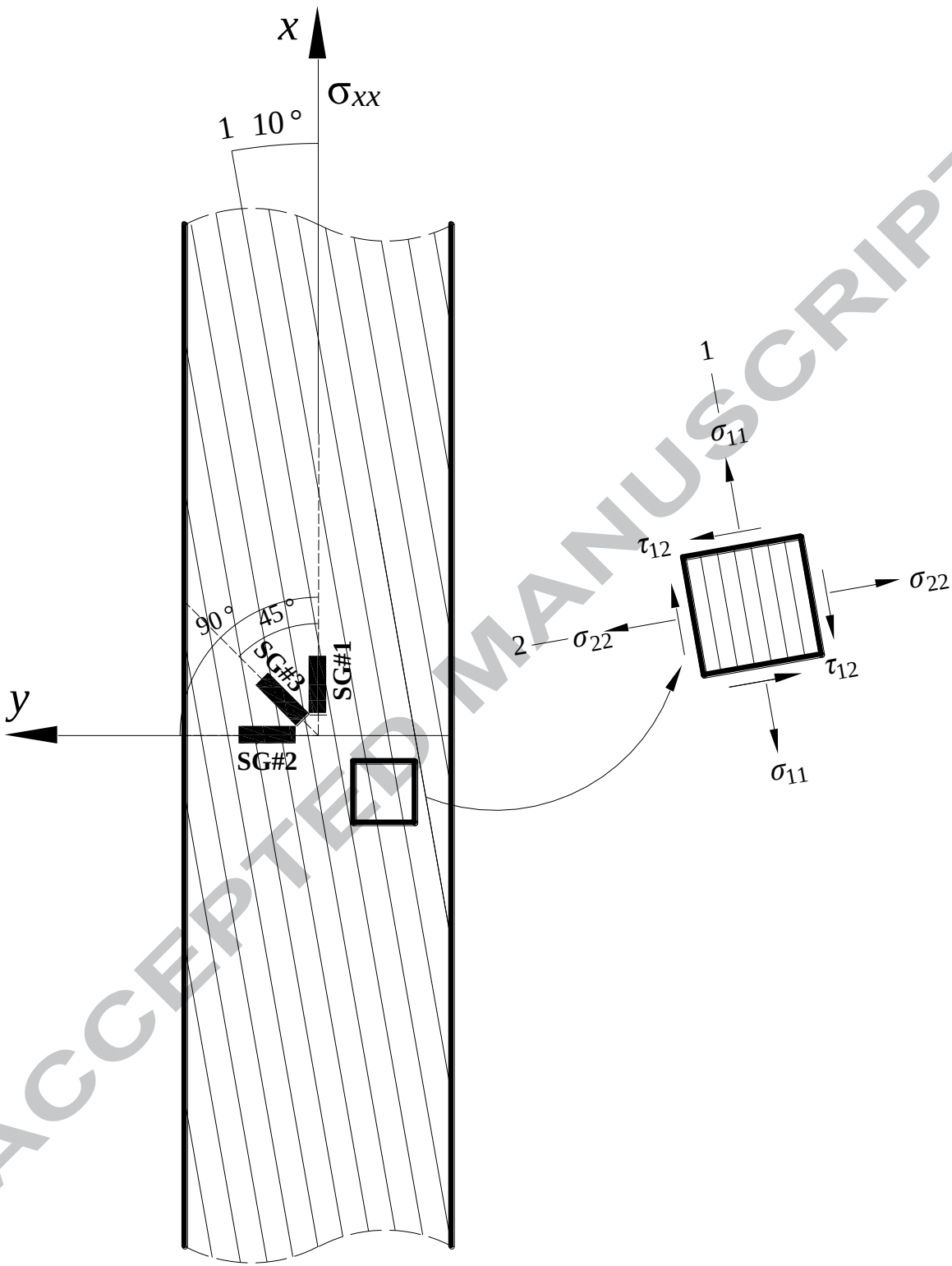

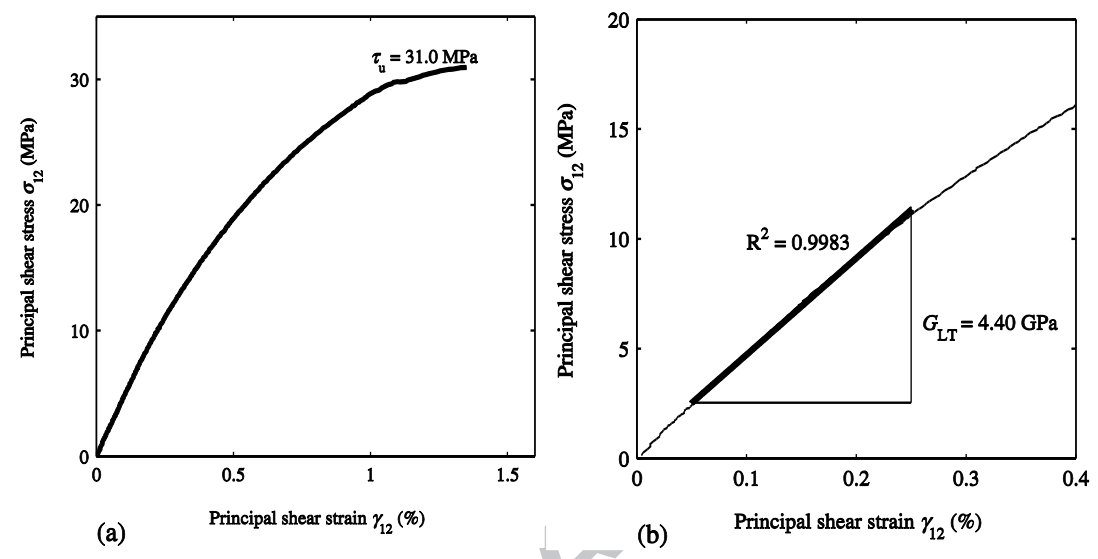
τ_u = 31.0 MPa
Principal shear stress σ_{12} (MPa)
Principal shear strain γ_{12} (%)
(a)
R^2 = 0.9983
G_{LT} = 4.40 GPa
Principal shear stress σ_{12} (MPa)
Principal shear strain γ_{12} (%)
(b)

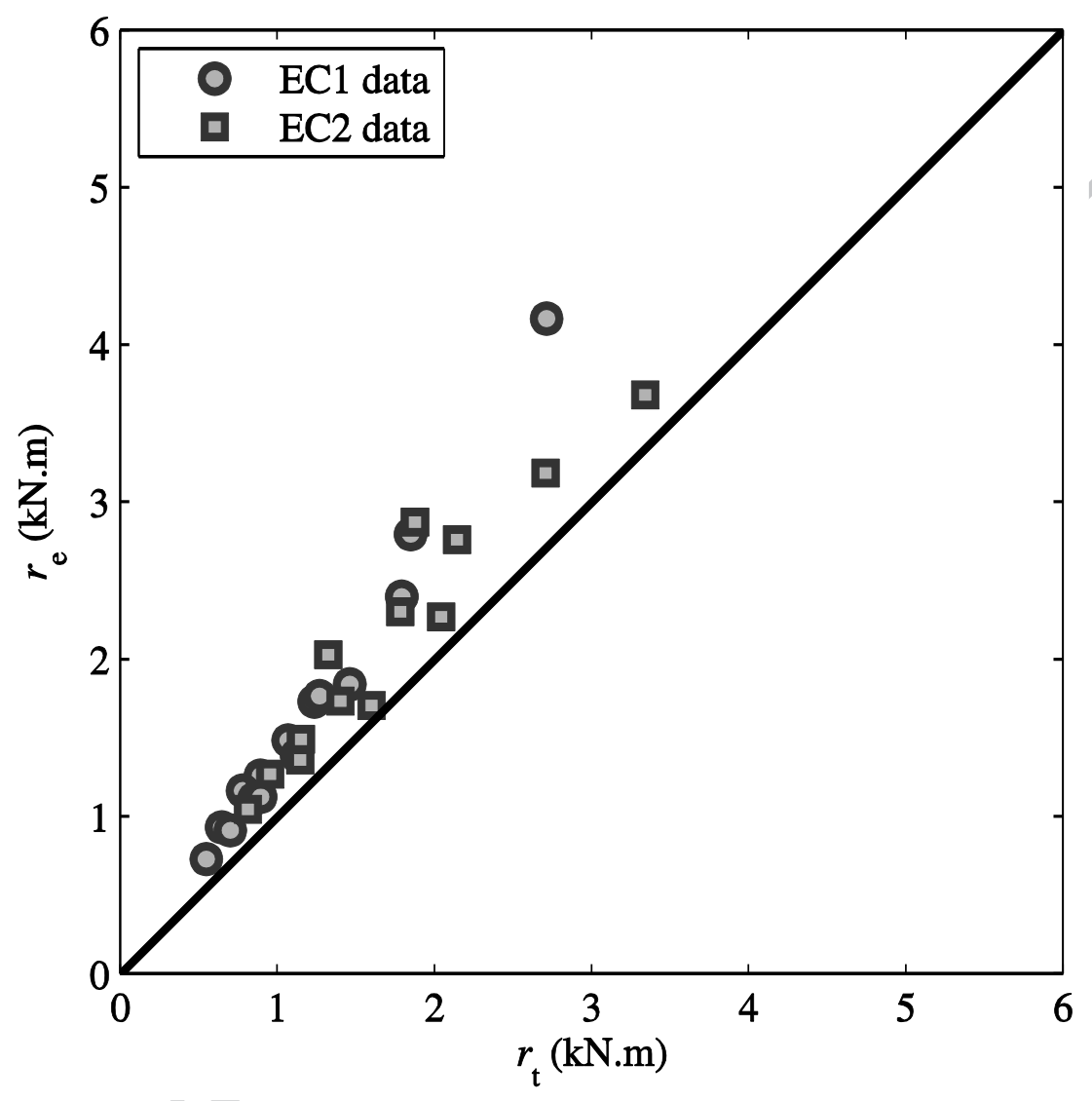
EC1 data
EC2 data
r_e (kN.m)
r_t (kN.m)
0
1
2
3
4
5
6

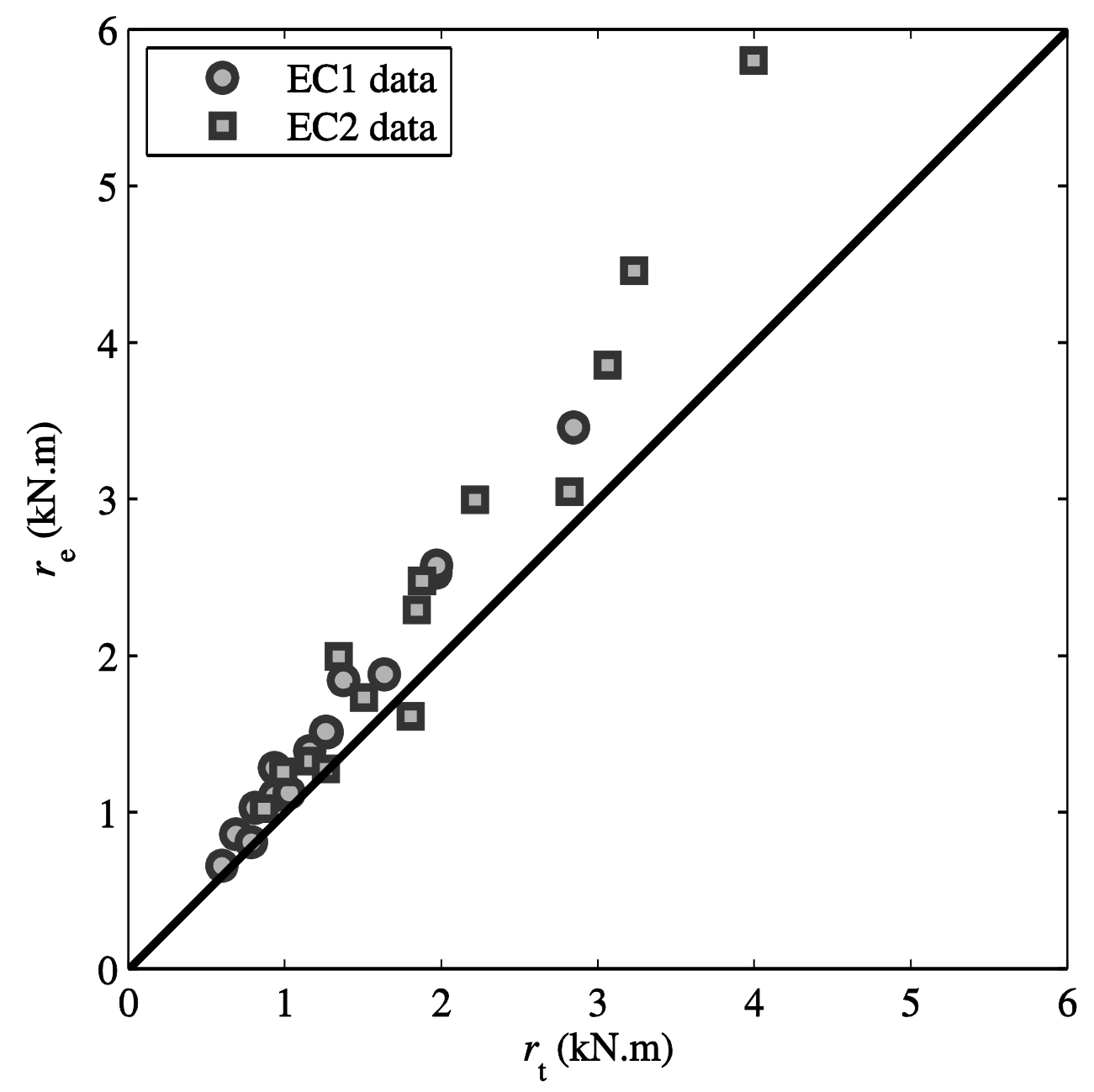
EC1 data
EC2 data
r_e (kN.m)
r_t (kN.m)
0
1
2
3
4
5
6

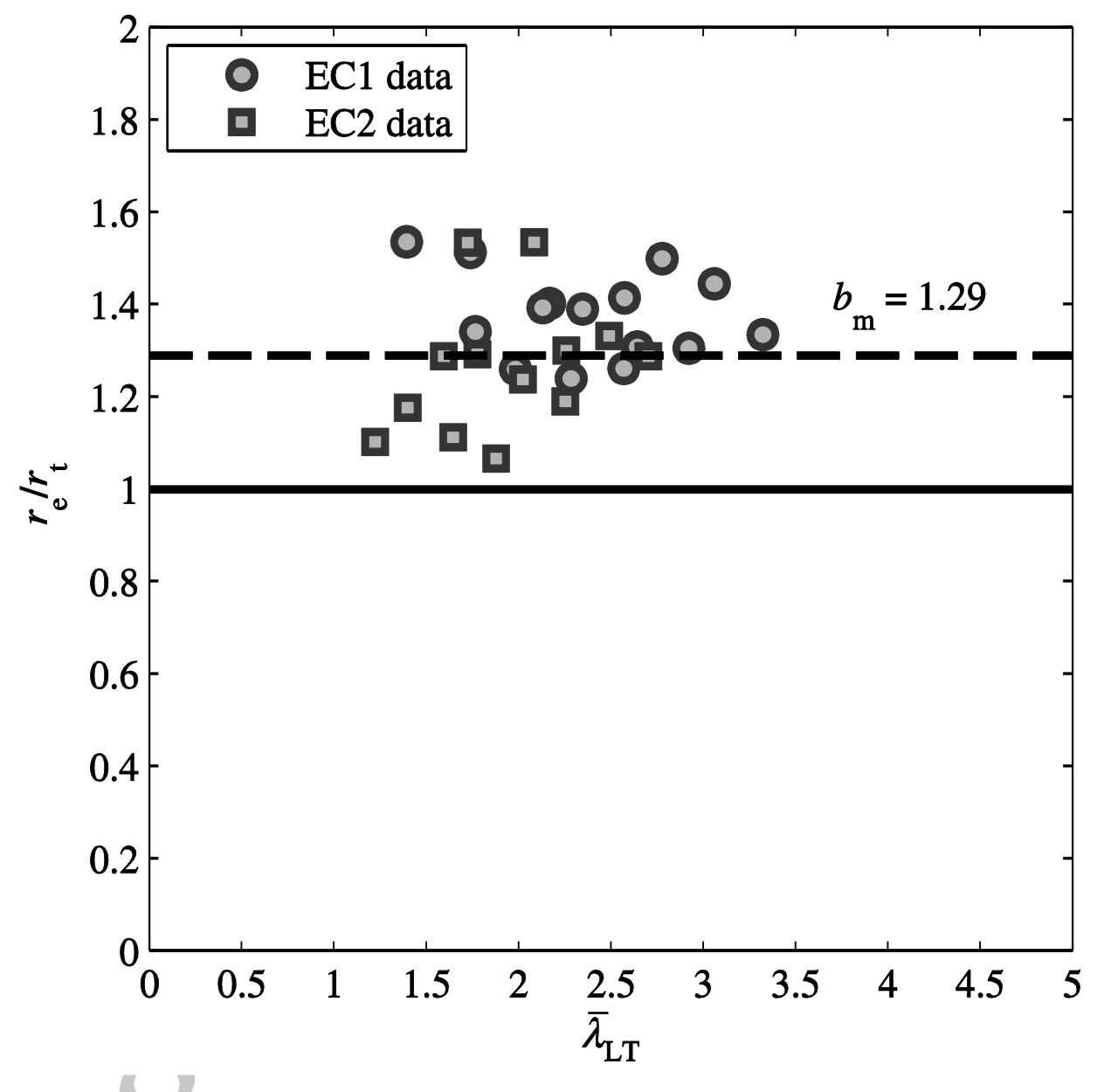
EC1 data
EC2 data
$b_m = 1.29$
r_e/r_t
$\bar{\lambda}_{LT}$
0
0.2
0.4
0.6
0.8
1
1.2
1.4
1.6
1.8
2
0
0.5
1
1.5
2
2.5
3
3.5
4
4.5
5

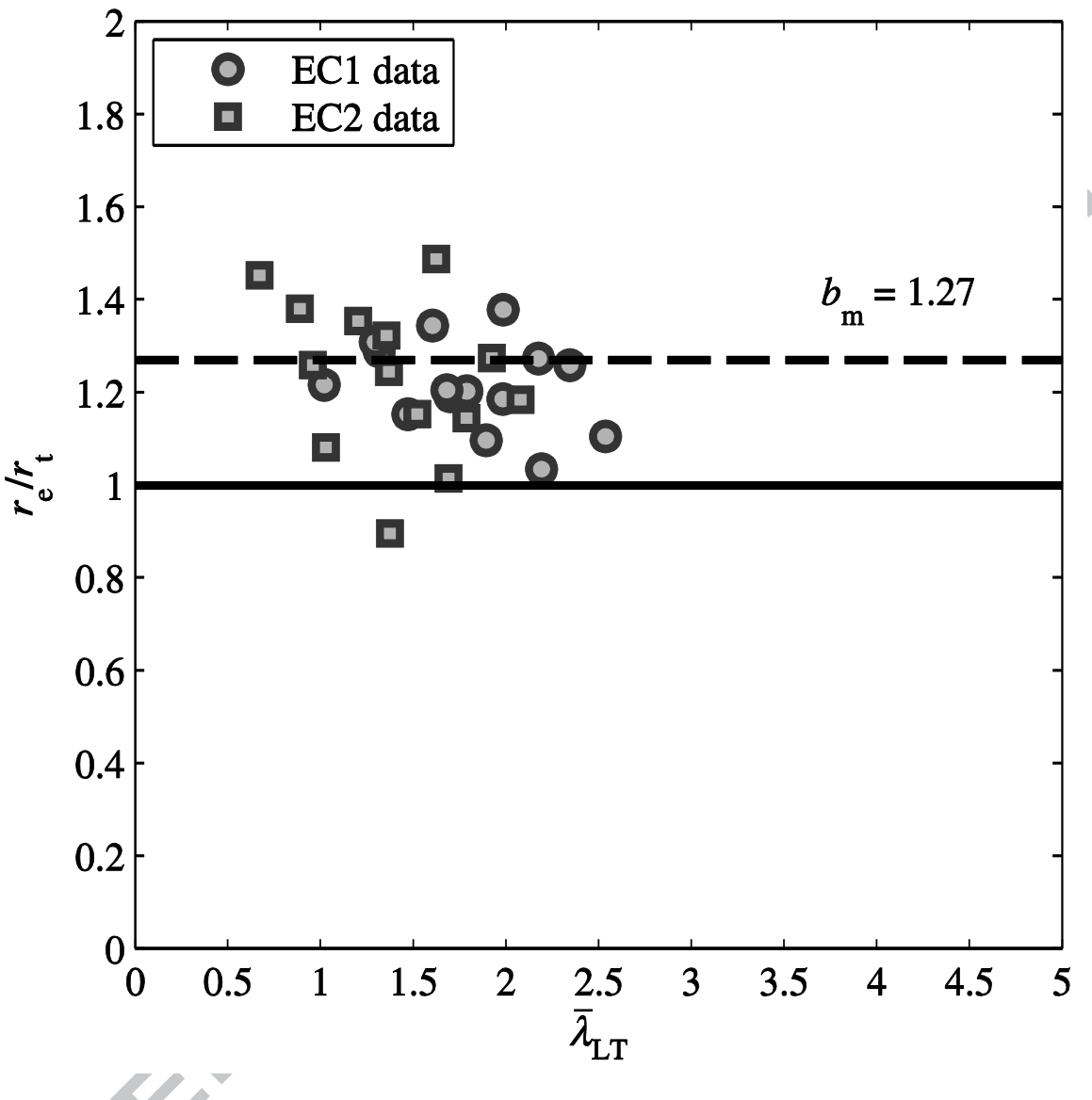
EC1 data
EC2 data
$b_m = 1.27$
r_e/r_t
$\bar{\lambda}_{LT}$
0
0.2
0.4
0.6
0.8
1
1.2
1.4
1.6
1.8
2
0
0.5
1
1.5
2
2.5
3
3.5
4
4.5
5

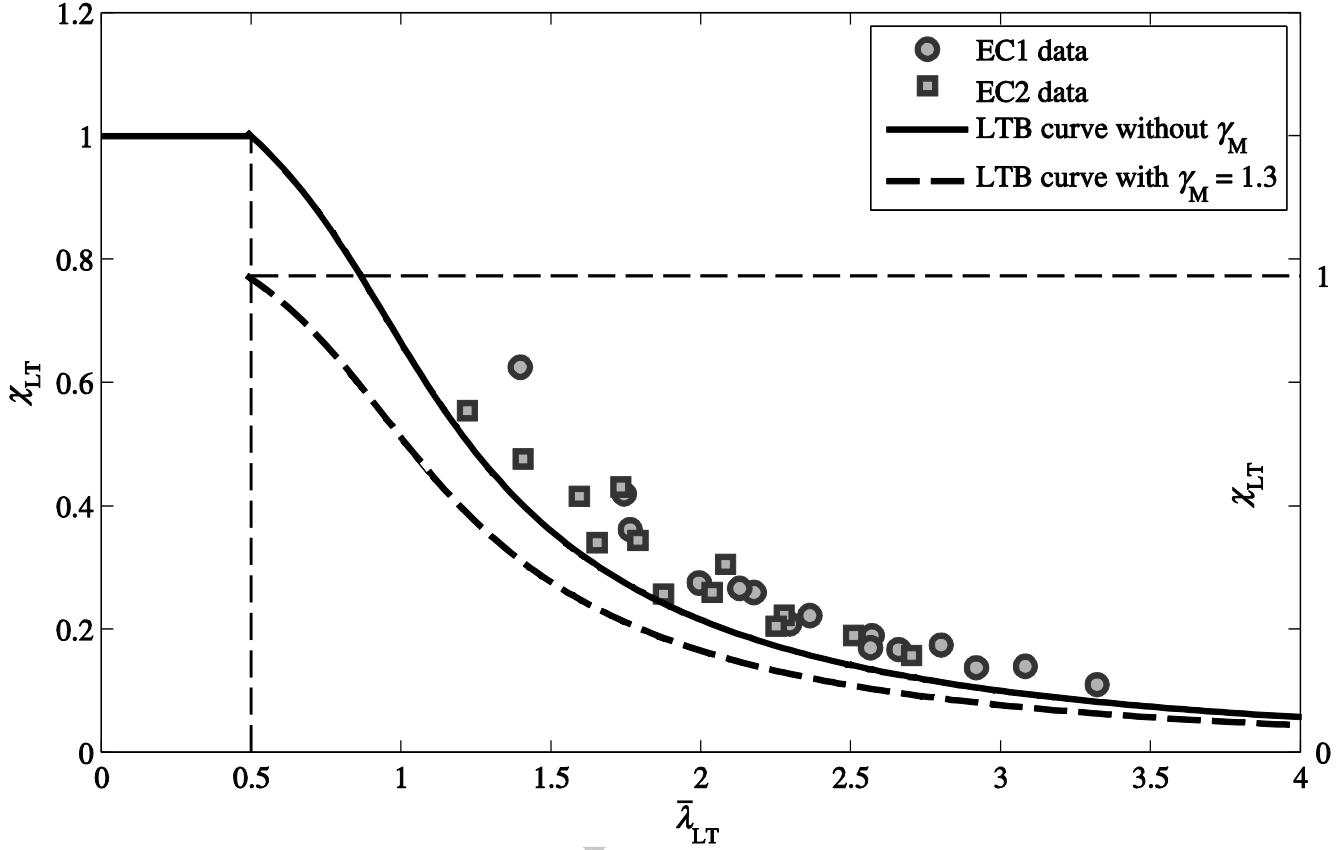
EC1 data
EC2 data
LTB curve without γ_M
LTB curve with $\gamma_M = 1.3$
χ_{LT}
$\bar{\lambda}_{LT}$
1.2
1
0.8
0.6
0.4
0.2
0
0.5
1
1.5
2
2.5
3
3.5
4

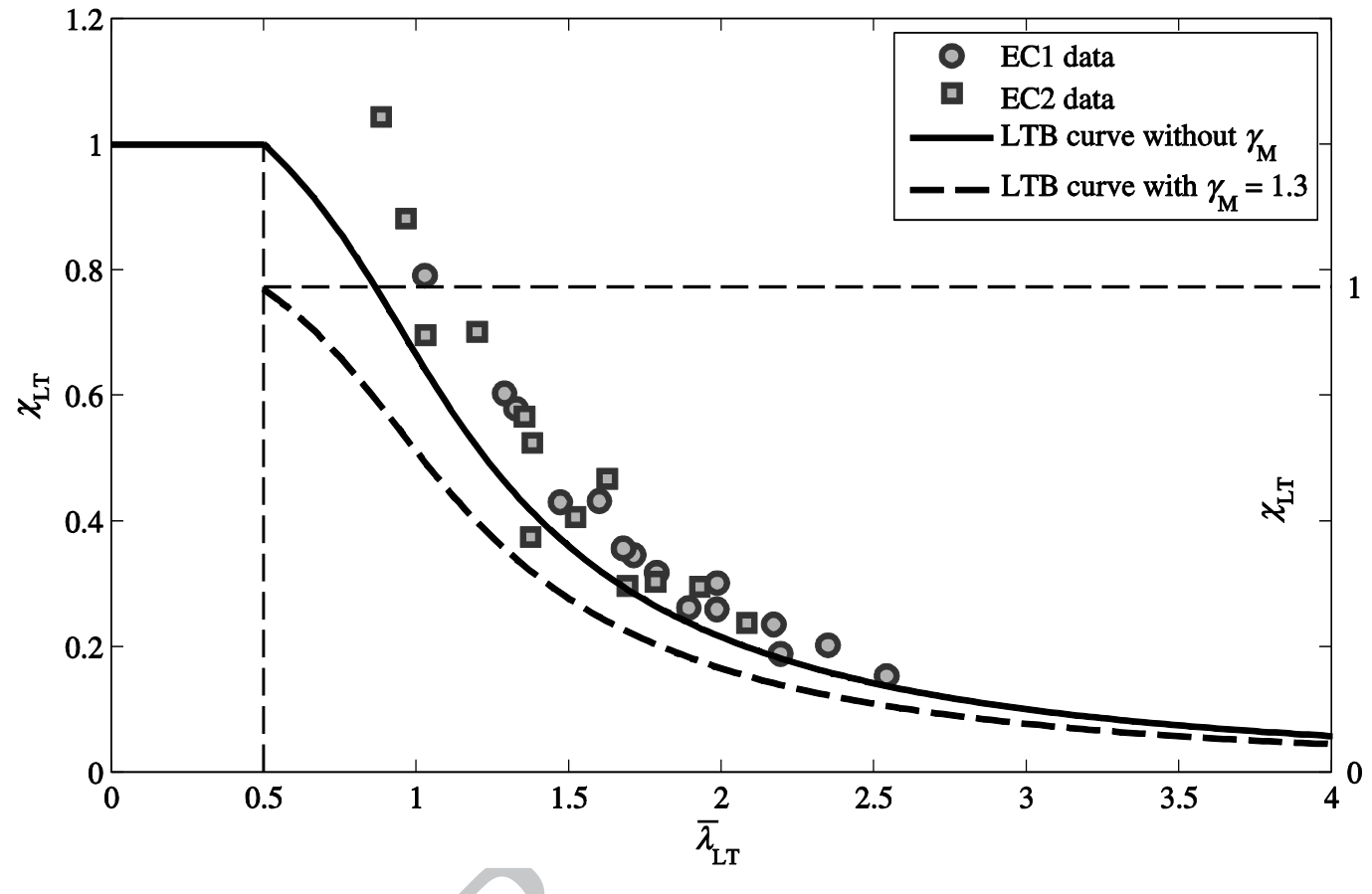
EC1 data
EC2 data
LTB curve without γ_M
LTB curve with $\gamma_M = 1.3$
χ_{LT}
$\overline{\lambda}_{LT}$
1.2
1
0.8
0.6
0.4
0.2
0
0.5
1.5
2
2.5
3
3.5
4

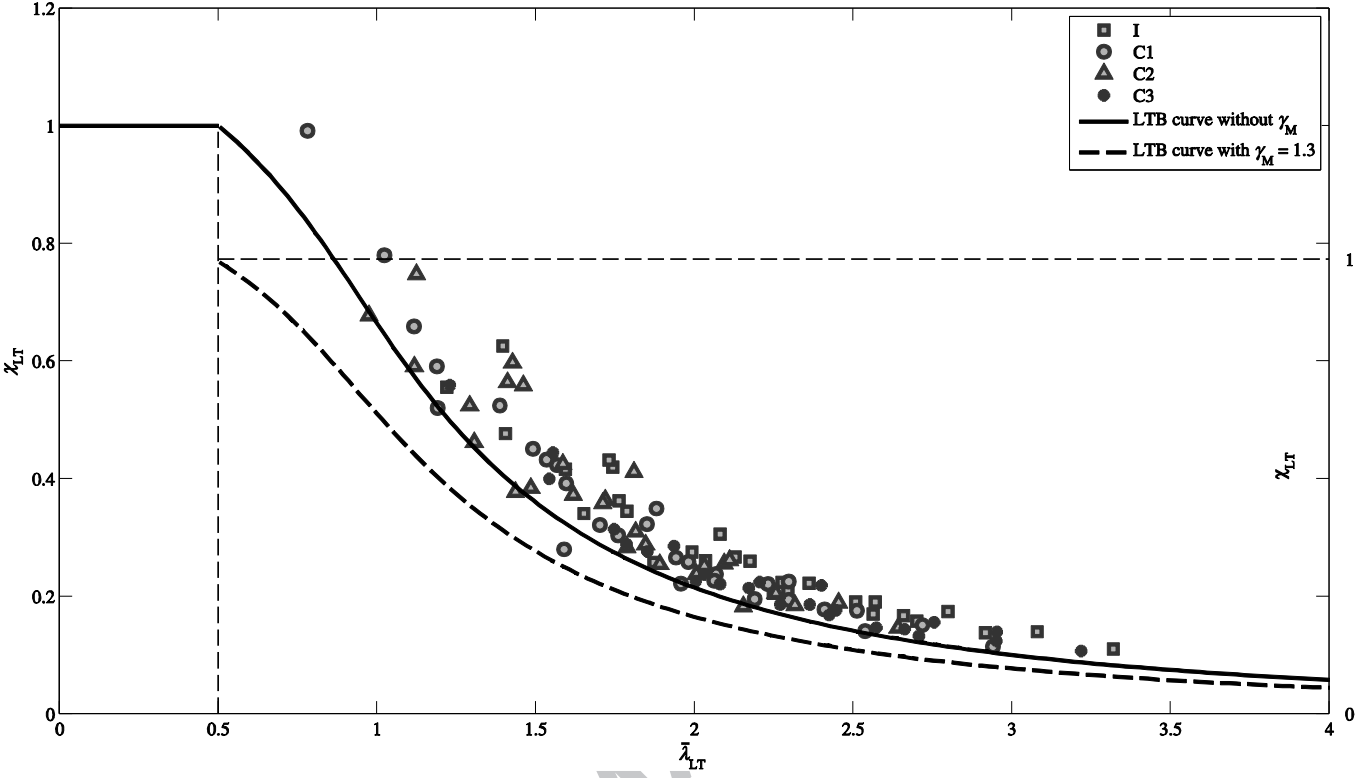
I
C1
C2
C3
LTB curve without γ_M
LTB curve with $\gamma_M = 1.3$
χ_{LT}
$\bar{\lambda}_{LT}$
1.2
1
0.8
0.6
0.4
0.2
0
0.5
1
1.5
2
2.5
3
3.5
4